Research Article | Vol. 26, No. 10 | 14 May 2018 | OPTICS EXPRESS A602
Optics EXPRESS

Optical and mechanical tolerances in hybrid concentrated thermal-PV solar trough

LILIANA RUIZ DIAZ,[1,*] BYRON COCILOVO,[1] ALEXANDER MILES,[1] WEI PAN,[2] PIERRE-ALEXANDRE BLANCHE,[1] AND ROBERT A. NORWOOD[1]

[1]*College of Optical Sciences, University of Arizona, 1630 E. University Blvd., Tucson, AZ, 85721, USA*
[2]*DWP Energy Solutions, LLC, 18110 SE 34th Street Building 4, Suite 480, Vancouver, WA, 98683, USA*
**ldiaz@optics.arizona.edu*

Abstract: Hybrid thermal-PV solar trough collectors combine concentrated photovoltaics and concentrated solar power technology to harvest and store solar energy. In this work, the optical and mechanical requirements for optimal efficiency are analyzed using non-sequential ray tracing techniques. The results are used to generate opto-mechanical tolerances that can be compared to those of traditional solar collectors. We also explore ideas on how to relieve tracking tolerances for single-axis solar collectors. The objective is to establish a basis for tolerances required for the fabrication and manufacturing of hybrid solar trough collectors.

OCIS codes: (350.6050) Solar energy; (080.2208) Fabrication, tolerancing; (220.1770) Concentrators.

References and links

1. M. Romero and A. Steinfeld, "Concentrating solar thermal power and thermochemical fuels," Energy Environ. Sci. **5**(11), 9234–9245 (2012).
2. D. Cocco, L. Migliari, and M. Petrollese, "A hybrid CSP–CPV system for improving the dispatchability of solar power plants," Energy Convers. Manage. **114**, 312–323 (2016).
3. X. Ju, C. Xu, X. Han, X. Du, G. Wei, and Y. Yang, "A review of the concentrated photovoltaic/thermal (CPVT) hybrid solar systems based on the spectral beam splitting technology," Appl. Energy **187**, 534–563 (2017).
4. A. Green, C. Diep, R. Dunn, and J. Dent, "High capacity factor CSP-PV hybrid systems," Energy Procedia **69**, 2049–2059 (2015).
5. H. Price, E. Lüpfert, D. Kearney, E. Zarza, G. Cohen, R. Gee, and R. Mahoney, "Advances in parabolic trough solar power technology," ASME. J. Sol. Energy Eng. **124**(2), 109–125 (2002).
6. M. A. Green, K. Emery, Y. Hishikawa, W. Warta, and E. D. Dunlop, "Solar cell efficiency tables (version 45)," Prog. Photovolt. Res. Appl. **23**(1), 1–9 (2015).
7. S. Kurtz, S. P. Philipps, A. W. Bett, and K. Horowitz, "Current status of concentrator photovoltaic (CPV) technology," Fraunhofer Institute for Solar Energy Systems / National Renewable Energy Laboratory. Report 1.3, TP-6A20–63916, (2017).
8. R. N. Clark, "Cassegrain telescopes: limits of secondary movement in secondary focusing," Appl. Opt. **15**(5), 1266–1269 (1976).
9. K. Shanks, N. Sarmah, K. S. Reddy, and T. Mallick, "The design of a parabolic reflector system with high tracking tolerance for high solar concentration," in *AIP Conf. Proc.* **1616**, 211 (2014).
10. L. Ruiz Diaz, B. Cocilovo, A. Miles, P. Blanche, W. Pan, and R. A. Norwood, "Tolerance analysis and characterization of hybrid thermal-PV solar trough prototype," *in Light, Energy and the Environment*, OSA Technical Digest (Optical Society of America, 2017), paper RW3B.6.
11. A. Miles, B. Cocilovo, B. Wheelwright, W. Pan, D. Tweet, and R. A. Norwood, "Designing spectrum-splitting dichroic filters to optimize current-matched photovoltaics," Appl. Opt. **55**(8), 1849–1853 (2016).
12. B. Wheelwright, W. Pan, and D. Tweet, "Solar Concentrator with Asymmetric Tracking-Integrated Optics," US patent 20160099675 A1, (2016).
13. R. C. Gee and E. K. May, "Solar thermal power and industrial heat: parabolic trough concentrating collectors components and system design," in *CRC Handbook of Energy Efficiency,* F. Kreith and R. E. West ed. (CRC Press, 1996).
14. M. Iqbal, *An Introduction to Solar Radiation* (Academic Press, 1983), Chap. 1.

1. Introduction

The use of concentrated solar power (CSP) and concentrated photovoltaic (CPV) technologies to collect and store solar energy has several advantages over traditional solar collectors [1]. The integration of these technologies in one system can result in increased solar power concentration, enhanced optical efficiency, and better dispatchability of solar energy through

#320491 https://doi.org/10.1364/OE.26.00A602
Journal © 2018 Received 24 Jan 2018; revised 1 Apr 2018; accepted 2 Apr 2018; published 1 May 2018

Optics EXPRESS

thermal storage methods [2–4]. In this work, we have developed a hybrid thermal-PV solar energy collection system based on spectral beam splitting technology to increase the efficiency and exergy of solar plants, primarily for utility scale deployment, where typically hundreds of trough systems would be deployed to achieve megawatt level exergies.

Our hybrid system design combines CSP and CPV principles to collect, concentrate, and store solar energy. CSP systems are proficient at harvesting a broad portion of the solar spectrum by collecting focused sunlight as thermal energy which can be stored and used for dispatchable generation [5]. CSPs tend to be low cost, but their annual solar-to-electric efficiency tends to be lower than traditional flat c-Si PV systems (around 16% for CSPs and 22% for c-Si PV systems under standard test conditions) [6]. CPVs, on the other hand, use parabolic mirrors to concentrate light onto high efficiency photovoltaic cells [7]. CPVs are highly efficient over their finite absorption band (above 40% efficiency under controlled conditions have been reported) but the generated electricity cannot be easily stored, rendering them ineffective at night or when shadowed [7]. The thermal-PV solar trough merges the storage capability of CSP and the efficiency of CPV technology into a single device to generate and store energy at reasonable costs. Moreover, the use of micro-CPV cells allows a geometrical solar concentration ratio of nearly 1000x whereas conventional parabolic trough concentration ratios range from 15 to 80x [1,7].

As in any optical system, the alignment and positioning of the different components of the collector affect the throughput and transmission of the light. This is of utmost importance in solar collectors, where the goal is to limit losses as much as possible. There exist analytical tolerance studies for Cassegrain imaging systems [8] and studies using ray tracing techniques [9]. The use of non-sequential ray tracing to measure optical throughput allows us to take into account solar divergence as well as wavelength-dependent effects such as non-constant refractive index and Fresnel losses. In this work, we present a tolerance analysis for the opto-mechanical properties of our hybrid thermal-PV solar trough design using a non-sequential ray tracing approach. This is an expansion of our previously presented tolerance study [10].

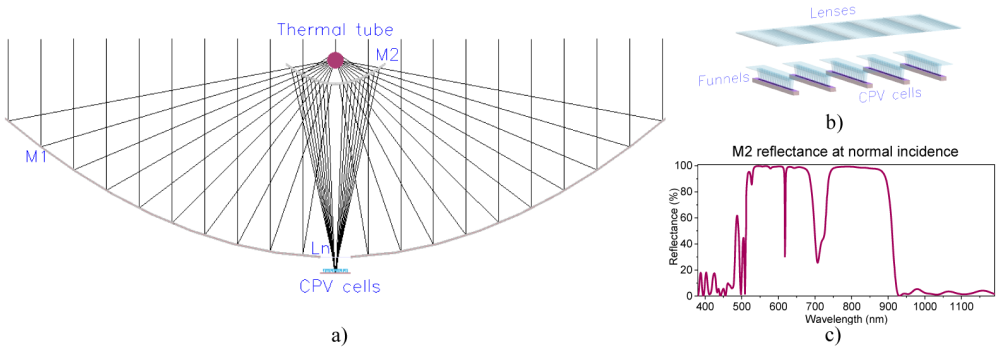

Fig. 1. Hybrid thermal-PV solar trough system: a) M1 collects the full solar spectrum and focuses it at the thermal tube while M2 reflects a fraction of the sunlight to the CPV cells, b) secondary concentrating optics module, and c) M2 dichroic design optimized for Tucson, AZ.

2. Hybrid thermal-PV solar trough

The hybrid thermal-PV solar trough system consists of a set of concentric cylindrical mirrors arranged in a Cassegrain configuration [Fig. 1(a)]. The primary mirror, M1, is a parabolic metallic reflector that collects the sunlight and concentrates it towards its focal line, where a vacuum insulated thermal tube is placed. The tube carries heat transfer fluid that heats up as the system tracks the sun. The secondary mirror, M2, is a hyperbolic reflector with an optimized dichroic filter on the front surface [Fig. 1(c)]. The dichroic filter has been designed to: (1) reflect the solar spectrum used by integrated dual-junction micro CPV cells and (2) transmit the remaining sunlight to heat the thermal tube. The details of the dichroic filter

Optics EXPRESS

design and optimization algorithms to achieve current-matching in the CPV cells can be found in our previous work [11]. To further increase the optical concentration, additional optical modules are placed at the secondary focus of M2 [Fig. 1(b)]. Each module tracks the solar elevation angle and is composed of a concentrating f/1 Fresnel lens, Ln, a glass plate with an anti-reflection coating, and a set of optical glass funnels bonded to the CPV cells [12].

The size and dimensions of the collector are scalable. For this design, we use standard mirror dimensions utilized in CSP industry. The full aperture of M1 is 5.0 m and the distance from its vertex to the thermal tube (the parabola focus, f_1) is 1.49 m. The Fresnel lenses are made of acrylic glass and have an aperture size of 100 x 230 mm and a 0.5° draft facet angle. The exit faces of the glass optical funnels are index matched to 5.0 x 5.5 mm CPV cells. Due to shadowing produced by M2, the maximum geometrical concentration ratio at the CPV cells is 965, which multiplied by the effective PV band, the PV energy conversion efficiency, the collector throughput, and the annualized solar irradiance incident on the collector aperture, results in an optical concentration equal to 138x. The average annual collection of Direct Normal Irradiance (DNI) by the CPV cells (PV/DNI) is 14.36% while the thermal exergy collection is 15.70%. Hence, our thermal-PV design has a total exergy efficiency of 30.06%.

3. Ray tracing simulations

For the simulations, the Standard Air Mass 1.5 (AM 1.5) solar spectrum was included in the modeled solar source, as well as the sun's divergence. Non-sequential optical effects were considered, including Fresnel losses, total internal reflection, absorption, stray light, and additional ray paths from secondary reflections. The collector mirrors were assumed to have reflectivity equal to aluminum for the optical collection, and equal to Schott B270 glass, for the thermal collection. The reflectivity, refractive index, and absorption values were taken from the internal library of Synopsys LightTools, the design ray tracing software used for this study.

In order to quantify the effects of shifting and tilting the mirrors from their ideal position, different misalignment scenarios were analyzed. The mirrors were shifted along the z-axis and x-axis and tilted by angles α and β about the y-axis and x-axis, respectively [Fig. 2]. For determining tracking accuracy, the whole system was rotated by θ_T about the y-axis. The optical surface quality of the mirrors was studied as well.

For the tolerance analysis, we focused on the collection of solar irradiance rather than on exergy and PV conversion. In this paper, the normalized amount of solar irradiance collected by the thermal tube is referred to as the thermal efficiency. The normalized irradiance received at the top of the CPV cells is referred to as the PV efficiency. Both quantities were simulated separately. The thermal tube was modeled as an absorbent cylindrical detector while the CPV cells as optical absorbers encapsulated in index-matched material bonded to the funnels.

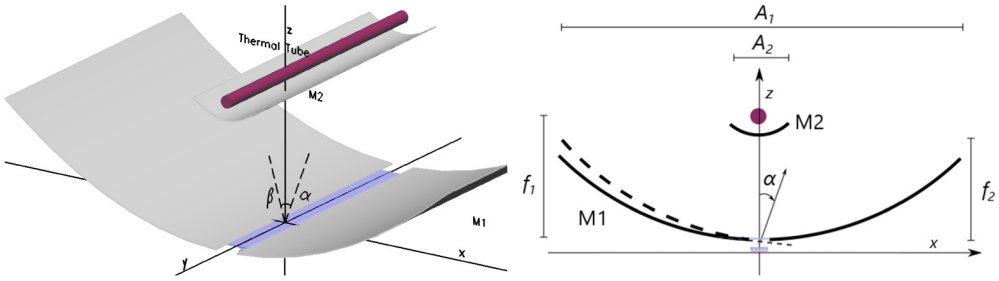

Fig. 2. Angle definitions: α represents the tilt angle about the y-axis while β is that about the x-axis. The mirrors are shifted along the z- and x-axis. The system is invariable along the y-axis.

In the thermal simulations, most of the light is transmitted through M2 but a small fraction of the DNI is directly reflected from the back of M2 and collected by the thermal tube. The normalized thermal efficiency is then defined as

Optics EXPRESS

$$E_T(\alpha,\beta,\theta_T,x,z)=\frac{C_1*I_{M1}(\alpha,\beta,\theta_T,x,z)+C_2*r*I_{M2}(\alpha,\beta,\theta_T,x,z)}{C_1*I_{M1}(0,0,0,0,0)+C_2*r*I_{M2}(0,0,0,0,0)} \quad (1)$$

where $I_{M1}(\alpha,\beta,\theta_T,x,z)$ is the irradiance, as a function of tolerance variables, collected by M1 and transmitted through M2. $I_{M2}(\alpha,\beta,\theta_T,x,z)$ is the irradiance directly reflected by M2 to the thermal tube. The constant C_1 is the normalized fraction of the collected PV band over the AM 1.5 spectrum and C_2 is equal to 1-C_1. The constant r is the ratio between the effective aperture of M2 and M1, A_1/A_2. The equation is normalized using the simulated irradiance values at ideal positions, $I_{M1}(0,0,0,0,0)$ and $I_{M2}(0,0,0,0,0)$. On the other hand, the normalized PV efficiency is simply $E_{PV} = I_{PV}(\alpha,\beta,\theta_T,x,z)/I_{PV}(0,0,0,0,0)$, where I_{PV} is the irradiance concentrated at the top of the CPV cells.

3.1 Mirror tolerance analysis

Simulation results for the position of the mirrors along the *x*-axis and *z*-axis are shown in Fig. 3. The PV efficiency is more severely affected than the thermal efficiency is by shifting effects due to the fact that for PV the light is reflected twice along the optical path. The thermal efficiency has a relatively large shifting tolerance of ± 62 mm and over ± 150 mm along the *z*-axis for M1 and M2 positions, respectively, and ± 60 mm and over ± 200 mm along the *x*-axis. Moving M2 has less effect on the thermal collection than moving M1, as most of the light collected by the thermal tube is transmitted through M2 as it is shown in Eq. (1). In comparison, the PV efficiency has ± 10 mm tolerance along the *z*-axis for both M1 and M2 positions, as moving M1 up is equivalent to moving M2 down along the optical axis. The PV efficiency along the *x*-axis is symmetric about the cylindrical axis and has a ± 10 mm and a ± 12 mm distance tolerance for M1 and M2 respectively.

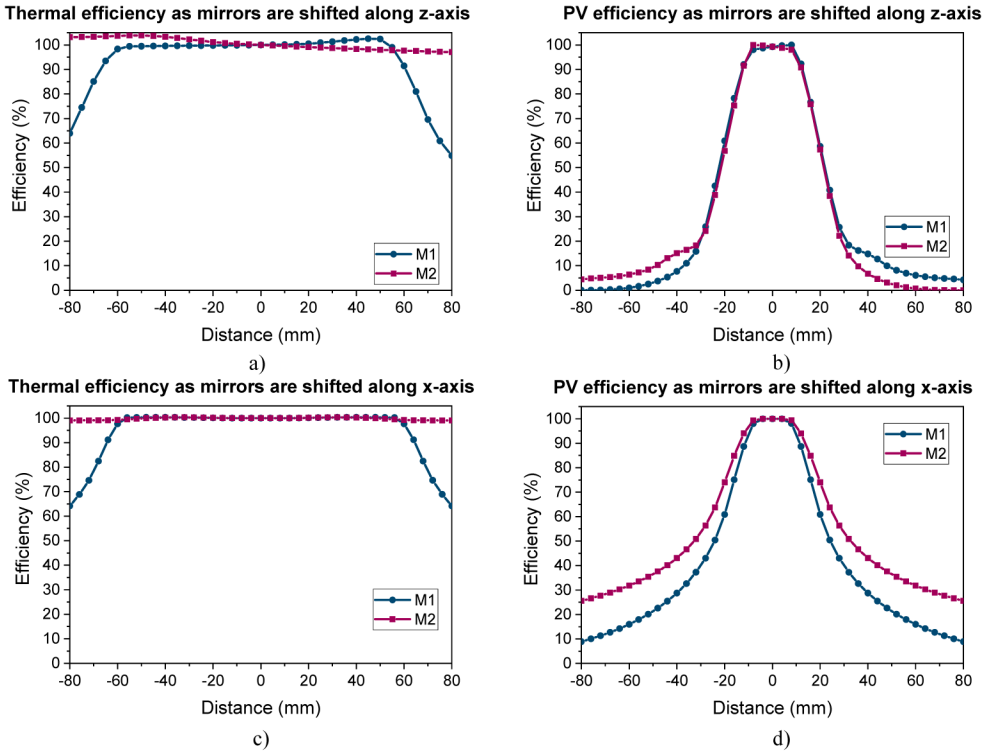

Fig. 3. Simulation results: a) normalized PV efficiency and b) thermal efficiency as M1 and M2 are shifted along the *z*-axis from their ideal positions and normalized c) PV efficiency and d) thermal efficiency as mirrors are moved in the *x*-direction.

Optics EXPRESS

In Fig. 4, the thermal and PV efficiencies are further analyzed by tilting the mirrors by α and β. As in the shifting case, the thermal efficiency is not significantly affected by unbalancing M2. Moreover, tilting tolerances about the x-axis tend to be more relaxed than those about the y-axis due to the cylindrical nature of the system. This is shown by having a ± 1.3° α and over ± 5° β tilting tolerance on M1 for the thermal collection [Fig. 4(b)]. For the PV collection, angular deviations due to tilting M1 by α are significantly larger than those produced by tilting M2 about the same direction due to the secondary reflection on M2. The PV efficiency has a 0.25° α tolerance for M1 and ± 1.2° α tolerance for M2 [Figs. 4(c)–4(d)]. For β misalignment, the system has a ± 0.6° tolerance for both M1 and M2, but the effect is more visible in the M2 case as only one segment of M1 was tilted in the simulations. In Fig. 4(d), the PV collection has a larger α than β tolerance. This happens as M2 acts as spherical mirror for small angle deviations and keeps focusing the light onto the CPV cells.

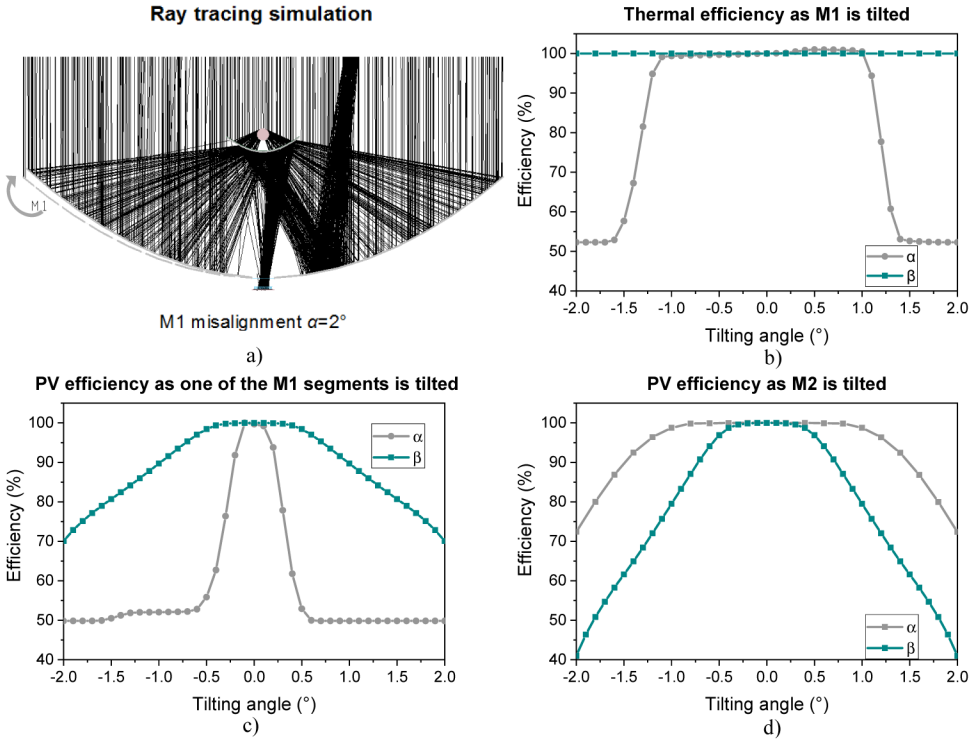

Fig. 4. Thermal and PV tolerances: a) ray tracing of M1 segment tilted by α = 2°, b) thermal efficiency as M1 is tilted by α and β, PV efficiency as c) M1 and d) M2 are tilted by α and β.

Losses due mirror surface scattering features were also studied. In an optical surface, the reflectance can be described as the addition of a diffuse and a specular component. In our simulations, the diffuse reflection was modeled as an ideal Lambertian scatterer while the specular reflection was modeled as Gaussian scatterer with a standard deviation m (in degrees) [Figs. 5(a)-5(b)]. As m increases, the specular component becomes more isotropic. A high specular reflector percentage also means that there is no Lambertian reflectance component. Losses due to material absorption were ignored as they are similar for all scatterers.

In Fig. 5(c), the PV efficiency for different scattering functions in M1 surface is shown. For low m values, the normalized efficiency is linearly proportional to the amount of specular content, thus a 96% near specular mirror will lose 4% of the incident sunlight. The losses increase as the Gaussian specular reflection deviates from the ideal specular case. For instance, surfaces with m = 0.2° will decrease the PV efficiency by 10% even if there is no

Optics EXPRESS

Lambertian diffuse component. The surface requirements for M2 are roughly half than those for M1 as the optical path is reduced.

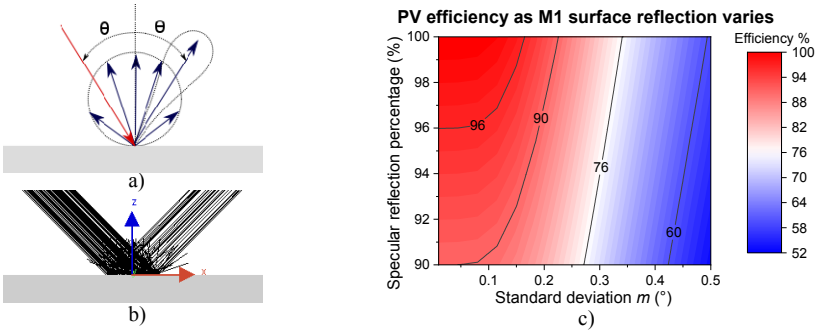

Fig. 5. Mirror surface quality: a) reflector with a diffuse Lambertian and a Gaussian specular component, b) mirror scatterer modeled in LightTools, and c) PV collection depends on M1 surface quality; high specular percentage and low *m* value have low scattering losses.

3.2 Tracking tolerance analysis

The solar tracking accuracy was also analyzed. The hybrid thermal-PV solar trough is designed to track the sun from east to west by rotating the whole system about the *y*-axis by θ_T. For these simulations, the system was misaligned by an angular deviation from the ideal tracking position. As in the previous cases, the tracking tolerance is tighter for the PV collection than for its thermal counterpart with ± 0.3° tracking tolerance for PV and ± 1.4° for the thermal collection [Figs. 6(a)–6(b)]. This information determines the tracking requirements.

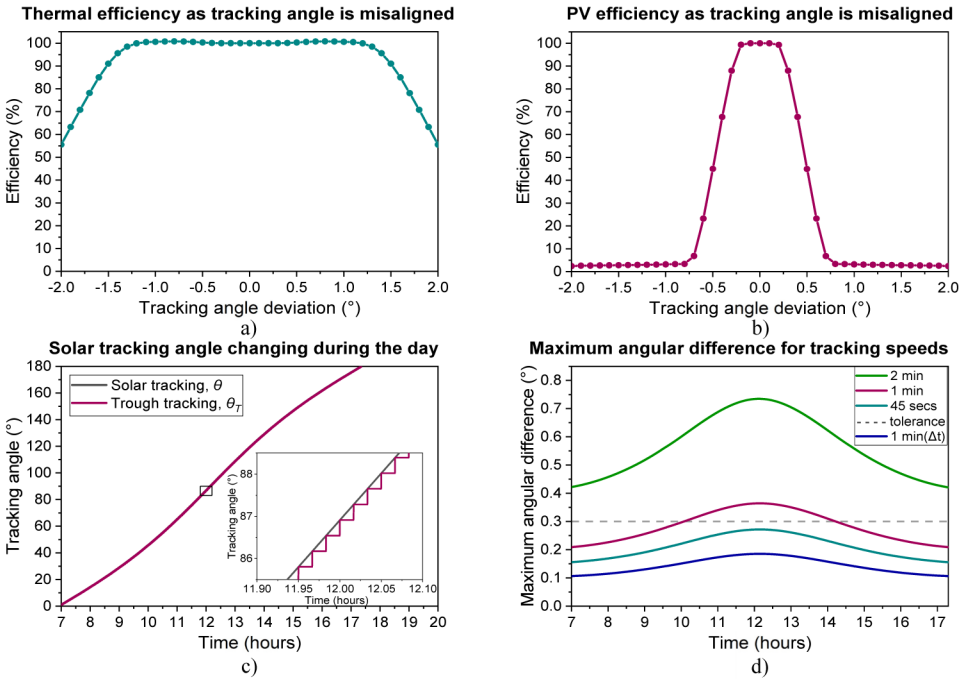

Fig. 6. Tracking accuracy: a) thermal and b) PV efficiency as tracking angle accuracy varies, c) solar tracking angle and a 1-min trough tracking rotation for Tucson, AZ on November 15th, and d) absolute maximum angular difference between θ and θ_T for different tracking speeds.

In traditional east-to-west CSP trough systems, the angle used to track the sun is

Optics EXPRESS

$$\theta = \arctan\left(-\sin\left(\phi\right)/\tan\left(\gamma\right)\right) \quad (2)$$

where ϕ is the solar azimuthal angle and γ is the sun's elevation angle [13]. These variables depend on the geolocation of the point of measurement, date, and time of the day. During winter time, θ changes rapidly since the day is shorter than during summer, and the trough must rotate faster to follow the sun's path. This can affect the tracking accuracy. In order to estimate θ for a winter day, standard solar equations were used to calculate ϕ and γ for Tucson, AZ [14]. In Fig. 6(c), the difference between θ and θ_T, the trough tracking angle, is shown. In this case, the trough rotates every minute to follow the sun's path and then remains in that position for a full minute. This generates a maximum tracking error right before the trough readjusts itself.

This maximum angular difference depends on the trough rotation frequency. A trough moving every 2 minutes will have larger maximum angular error than one that moves every 45 seconds [Fig. 6(d)]. The difference is higher at noon when θ changes faster. At noon, a 1-min trough tracking produces more angular error than the recommended tracking tolerance for our hybrid system (± 0.3°). A way to solve this issue is by tracking the sun $\Delta t = t_r/2$ ahead of time, where t_r is the tracking rotation time of the trough. This way the tracking angular difference is distributed and the maximum angular difference is halved. In this case, tracking every 1 minute or less assures that the system is within the tracking tolerance. This technique can be applied to any single-axis tracking solar collector.

4. Conclusions

A summary of the opto-mechanical tolerances is shown in Table 1. The ray tracing simulations indicate that our hybrid thermal-PV solar trough system has smaller tilting tolerances about the x-axis (θ_T and α) than about the y-axis (β). The PV irradiance collection is more severely affected by tilting and shifting effects in mirrors than its thermal counterpart. This is due to the secondary reflection on M2, but also because the CPV collection area is much smaller than the thermal tube surface area. Thus our system has tighter mechanical tolerances than systems that only utilize one concentrating mirror or have low solar concentration. The mirror surface quality was also studied. The presence of a diffuse Lambertian component linearly reduces the irradiance collection due to homogenous scattering losses. The losses are significantly increased if the specular reflection has a Gaussian profile with standard deviation greater than 0.2°. Our hybrid solar trough provides high solar concentration with suitable spectrum for multi-junction CPV cells. In order to maintain maximum concentration during the day, the system must be within tracking tolerances. This is determined by the PV irradiance collection as the thermal collection has relaxed tracking tolerances. Nonetheless, the tracking requirements can be relieved by tracking the sun ahead of time.

Table 1. Thermal and PV tolerances for 5.0 m solar hybrid trough system

	Thermal		PV	
Variable (±)	M1	M2	M1	M2
x (mm)	60	>200	10	12
z (mm)	62	>150	10	10
α (°)	1.3	>5	0.25	1.2
β (°)	5	>5	0.6	0.6
θ_T (°)	1.4		0.3	

Funding

U.S. Department of Energy (DE-AR0000830).